Towards Bounding-Box Free Panoptic Segmentation

Ujwal Bonde[1] Pablo F. Alcantarilla[1] Stefan Leutenegger[1,2]
[1] SLAMcore Ltd. [2] Imperial College London
firstname@slamcore.com

Abstract

In this work we introduce a new bounding-box free network (BBFNet) for panoptic segmentation. Panoptic segmentation is an ideal problem for a bounding-box free approach as it already requires per-pixel semantic class labels. We use this observation to exploit class boundaries from an off-the-shelf semantic segmentation network and refine them to predict instance labels. Towards this goal BBFNet predicts coarse watershed levels and use it to detect large instance candidates where boundaries are well defined. For smaller instances, whose boundaries are less reliable, BBFNet also predicts instance centers by means of Hough voting followed by mean-shift to reliably detect small objects. A novel triplet loss network helps merging fragmented instances while refining boundary pixels. Our approach is distinct from previous works in panoptic segmentation that rely on a combination of a semantic segmentation network with a computationally costly instance segmentation network based on bounding boxes, such as Mask R-CNN, to guide the prediction of instance labels using a Mixture-of-Expert (MoE) approach. We benchmark our non-MoE method on Cityscapes and Microsoft COCO datasets and show competitive performance with other MoE based approaches while outperfroming exisiting non-proposal based approaches. We achieve this while been computationally more efficient in terms of number of parameters and FLOPs. Video results are provided here https://blog.slamcore.com/reducing-the-cost-of-understanding

1. Introduction

Panoptic segmentation is the joint task of predicting semantic scene segmentation together with individual instances of objects present in the scene. Historically this has been explored under different umbrella terms of scene understanding [43] and scene parsing [37]. In [17], Kirillov *et al*. coined the term and gave a more concrete definition by including Forsyth *et al*. [11] suggestion of splitting the objects categories into *things* (countable objects like persons, cars, etc.) and *stuff* (uncountable like sky, road, etc.) classes. While *stuff* classes require only semantic label prediction, *things* need both the semantic and the instance labels. Along with this definition, *Panoptic Quality* (PQ) measure was proposed to benchmark different methods. Since then, there has been a more concentrated effort towards panoptic segmentation with multiple datasets [7, 23, 25] supporting it.

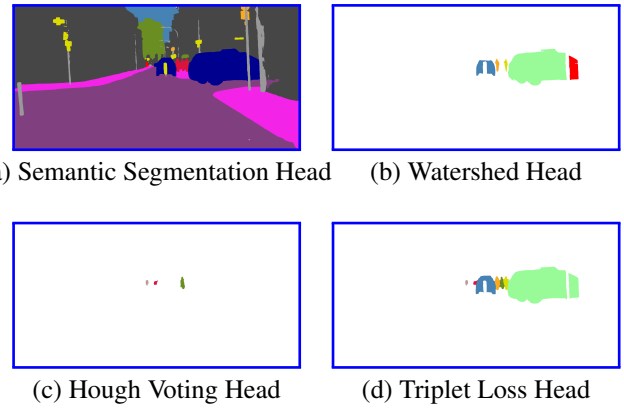

(a) Semantic Segmentation Head (b) Watershed Head

(c) Hough Voting Head (d) Triplet Loss Head

Figure 1. BBFNet gradually refines the class boundaries of the semantic segmentation network to predict panoptic segmentation. The Watershed head detects candidates for large instances whereas the Hough voting head detects small object instances. The Triplet Loss network refines and merges the detection to obtain the final instance labels.

Existing methods address this as a Multi-Task Learning (MTL) problem with different branches (or networks) used to predict the instance and scene segmentation. Traditionally these methods use completely separate instance and scene segmentation networks although more recently some works propose sharing a common feature backbone for both networks [16, 28]. Using a Mixture-of-Experts (MoE) approach the outputs are combined either heuristically or through another sub-network. In this work we show that instance information already exists in a semantic segmentation network. To support this we present *Bounding-Box Free Network* (BBFNet) which can be added to the

head of any off-the-shelf semantic segmentation network. By gradually refining the class boundaries predicted by the base network, BBFNet predicts both the *things* and *stuff* information in a scene. Without using MoE our method produces comparable results to existing approaches while being computationally efficient. Furthermore, the different sub-modules of BBFNet are end-to-end trainable while the base network requires no extra information.

An additional benefit of our proposed method is that we do not need bounding-box predictions. While bounding-box detection based approaches have been popular and successful, they require predicting auxiliary quantities like scale, width and height which do not directly contribute to instance segmentation. Furthermore, the choice of bounding-boxes for object-detection had been questioned in the past [31]. We believe panoptic segmentation to be an ideal problem for a bounding-box free approach since it already contains structured information from semantic segmentation. To achieve this we exploit previous works in non-proposal based methods for instance segmentation [3, 5, 26]. Based on the output of a semantic segmentation network, BBFNet first detects noisy and fragmented large instance candidates using a watershed-level prediction head (see Fig. 1). These candidate regions are clustered and their boundaries improved with a novel triplet loss based head. The remaining smaller instances, with unreliable boundaries, are detected using a Hough voting head that predicts the offsets to the center of the instance. Mean-shift clustering followed by vote back-tracing is used to reliably detect the smaller instances.

To summarise, we present BBFNet for panoptic segmentation which a bounding-box free end-to-end trainable non-MoE approach for panoptic segmentation network that does not use the output of any instance segmentation or detection network while outperforming existing non-proposal based methods. The next section briefly describes the related work in panoptic and instance segmentation. In §3 we introduce BBFNet and explain its various components along with its training and inference steps. §4 introduces the datasets used in our experiments and briefly describes the different metrics used for benchmarking panoptic segmentation. Implementation details are given in §4.1. Using ablation studies along with qualitative results we show the advantages of each of its components. Qualitative and quantitative results are presented in we §4.3 and used to benchmark BBFNet against existing MoE based approaches.

2. Related Work

Despite the recent introduction of panoptic segmentation there have already been multiple works attempting to address this [9, 19, 21, 41]. This is in part due to its importance to the wider community, success in individual subtasks of instance and semantic segmentation and publicly available datasets to benchmark different methods. We review related work and tasks here.

Panoptic Segmentation: Current works in panoptic segmentation are built upon a similar template of MTL followed by MoE. In [17], the authors use separate networks for semantic segmentation (*stuff*) and instance segmentation (*things*) with a heuristic MoE fusion of the two results for the final prediction. Realising the duplication of feature extractors in the two related tasks, [16, 19, 21, 28, 41] propose using a single backbone feature extractor network. This is followed by separate branches for the two sub-tasks (MTL) with a heuristic or learnable MoE head to combine the results. While panoptic Feature Pyramid Networks (FPN) [16] uses Mask R-CNN [13] for the *things* classes and fills in the *stuff* classes using a separate FPN branch, UPSNet [41] combines the resized logits of the two branches to predict the final output. In AUNet [21], attention masks predicted from the Region Proposal Network (RPN) and the instance segmentation head help fusing the results of the two tasks. Instead of relying only on the instance segmentation branch, TASCNet [19] predicts a coherent mask for the *things* and *stuff* classes using both branches. This is later filled with the respective outputs. All these methods rely on Mask R-CNN [13] for predicting *things*. Mask R-CNN is a two-stage instance segmentation network which uses a RPN to predict initial candidates for instance. The proposed candidates are either discarded or refined and a separate head produces segmentation for the remaining candidates. The two-stage, serial approach makes Mask R-CNN accurate albeit computationally expensive thus slowing progress towards real-time panoptic segmentation.

In FPSNet [9] the authors replace Mask R-CNN with a computationally less expensive detection network, RetinaNet [22], and use its output as a soft attention masks to guide the prediction of *things* classes. This trade off is at a cost of considerable reduction in accuracy. Furthermore RetinaNet still uses bounding-boxes for predicting *things*. In [35] the detection network is replaced with an object proposal which predicts instance candidates. Similarly, in [38] the authors predict the direction to the center and replace bounding box detection with template matching using these predicted directions as a feature. Instead of template matching, [2, 20] use a dynamically initiated conditional random field graph from the output of an object detector to segment instances. In [12], graph partioning is performed on an affinity pyramid computed within a fixed window for each pixel. In comparison, our work predicts *things* by refining the segmentation boundaries that can be obtained from any segmentation network.

Instance segmentation: Traditionally predicting instance segmentation masks relied on obtaining rough boundaries

followed by refining them [18, 34]. With the success of deep neural networks in predicting object proposals [30, 32], and the advantages of an end-to-end learning method, proposal based approaches have become more popular. Recent works have suggested alternatives to predicting proposals in an end-to-end trainable network. As these are most relevant to our work, we only review these below.

In [3], the authors propose predicting quantised watershed energies [39] using a Deep Watershed Transform network (DWT). Connected-components on the second-lowest watershed energy level are used to predict the instance segments. While this does well on large instances it suffers on small and thin instances. Moreover, fragmented regions of occluded objects end up being detected as different instances. In comparison, [5] embed the image into a transformed feature space where pixels of the same instance cluster together and pixels of different instances are pushed apart. While this method is not affected by object fragmentation, poor clustering often leads to either clustering multiple objects as single instance (under-segmentation) or segmenting large objects into multiple instances (over-segmentation). In [27], the authors try to address this by using variable clustering bandwidths predicted by the network. In this work, we observe the complementary advantages of these methods and exploit it towards our goal of an accurate, bounding-box free panoptic segmentation.

Semantic Boundaries: In addition to above, a parallel body of work deals with detection of object boundaries. In [1] the authors focus on detecting accurate object boundaries by explicitly reasoning about annotation noise. Using a new *semantic boundary thinning layer* the class boundaries are better localised. Boundaries, however, belong to multiple objects (two or more) and this fact is used to improve edge prediction in [15]. Here they explicitly condition boundaries on multiple objects to better segment objects. Either of these works could be incorporated to improve panoptic segmentation methods including ours.

3. Panoptic Segmentation

In this section we introduce our non-bounding box approach to panoptic segmentation. Fig. 2 shows the various blocks of our network and Table 1 details the main components of BBFNet. The backbone semantic segmentation network consists of a ResNet50 followed by an FPN [36]. In FPN, we only use the P2, P3, P4 and P5 feature maps which contain 256 channels each and are $1/4$, $1/8$, $1/16$ and $1/32$ of the original scale respectively. Each feature map then passes through the same series of eight deformable convolution blocks [8]. Intermediate features after every couple of deformable convolutions are used to predict semantic segmentation (§3.1), Hough votes (§3.2), watershed energies (§3.3) and features for the triplet loss [40] network. We first explain each of these components and their corresponding training loss. In (§3.5) we explain our training and inference steps. Through ablation studies we show the advantages of each block in (§4.2).

3.1. Semantic Segmentation

The first head in BBFNet is used to predict semantic segmentation. This allows BBFNet to quickly predict *things* (C_{things}) and *stuff* (C_{stuff}) labels while the remainder of BBFNet improves *things* boundaries using semantic segmentation features F_{seg}. The loss function used to train semantic segmentation is a per-pixel cross-entropy loss given by:

$$L_{ss} = \sum_{c \in \{C_{stuff}, C_{thing}\}} y_c \, \log(p_c^{ss}), \tag{1}$$

where y_c and p_c^{ss} are respectively the one-hot ground truth label and predicted softmax probability for class c.

3.2. Hough Voting

The Hough voting head is similar to the semantic segmentation head and is used to refine F_{ss} to give Hough features F_{hgh}. These are then used to predict offsets for the center of each *things* pixel. We use a $tanh$ non-linearity to squash the predictions and obtain normalised offsets ($\hat{X}_{\text{off}}$ and $\hat{Y}_{\text{off}}$). Along with the centers we also predict the uncertainty in the two directions (σ_x and σ_y) making the number of predictions from the Hough voting head equal to $4 \times C_{things}$. The predicted center for each pixel (x, y), is then given by:

$$\begin{aligned} \hat{X}_{\text{center}}(x,y) &= x + \hat{X}_{\text{off}}^{C(x,y)}(x,y), \\ \hat{Y}_{\text{center}}(x,y) &= y + \hat{Y}_{\text{off}}^{C(x,y)}(x,y), \end{aligned} \tag{2}$$

where C is the predicted class.

Hough voting is inherently noisy [4] and requires clustering or mode seeking methods like mean-shift [6] to predict the final object centers. As instances could have different scales, tuning clustering hyper-parameters is difficult. For this reason we use Hough voting primarily to detect small objects and to filter predictions from other heads. We also observe that the dense loss from the Hough voting head helps convergence of deeper heads in our network.

The loss for this head is only for the *thing* pixels and is given by:

$$\begin{aligned} L_{hgh} = w\Big(\frac{(X_{\text{off}} - \hat{X}_{\text{off}})^2}{\sigma_x} + \frac{(Y_{\text{off}} - \hat{Y}_{\text{off}})^2}{\sigma_y}\Big) \\ -\frac{1}{2}\Big(\log(\sigma_x) + \log(\sigma_y)\Big), \end{aligned} \tag{3}$$

where X_{off} and Y_{off} are ground truth offsets and w is the per pixel weight. To avoid bias towards large objects, we inversely weigh the instances based on the number of pixels.

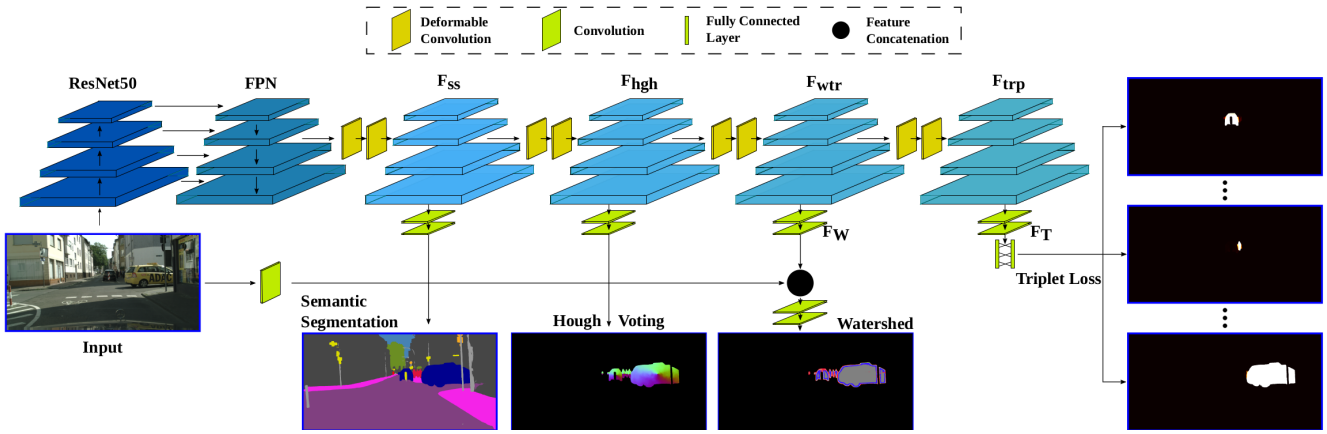

Figure 2. BBFNet gradually refines the class boundaries of the backbone semantic segmentation network to predict panoptic segmentation. The watershed head predicts quantized watershed levels (shown in different colours) which is used to detect large instance candidates. For smaller instances we use Hough voting with fixed bandwidth. The output shows offsets (X_{off}, Y_{off}) colour-coded to represent the direction of the predicted vector. Triplet head refines and merges the detection to obtain the final instance labels. We show the class probability (colour-map *hot*) for different instances with their center pixels used as f_a. Table 1 lists the components of individual heads while §3 explains them in detail.

This allows it to accurately predict the centers for objects of all sizes. Note that we only predict the centers for the visible regions of an instance and do not consider its occluded regions.

3.3. Watershed Energies

Our watershed head is inspired from DWT [3]. Similar to that work, we quantise the watershed levels into fixed number of bins ($K = 4$). The lowest bin ($k = 0$) corresponds to background and regions that are within 2 pixels inside the instance boundary. Similarly, $k = 1$, $k = 2$ are for regions that are within 5 and 15 pixels away from the instance boundary, respectively, while $k = 3$ is for the remaining region inside the instance.

In DWT, the bin corresponding to $k = 1$ is used to detect large instance boundaries. While this does reasonably well for large objects, it fails for smaller objects producing erroneous boundaries. Furthermore, occluded instances that are fragmented cannot be detected as a single object. For this reason we use this head only for predicting large object candidates which are filtered and refined using predictions from other heads.

Due to the fine quantisation of watershed levels, rather than directly predicting the upsampled resolution, we gradually refine the lower resolution feature maps while also merging higher resolution features from the backbone semantic segmentation network. F_{hgh} is first transformed into F_{wtr} followed by further refining into F_W as detailed in table 1. Features from the shallowest convolution block of ResNet are then concatenated with F_W and further refined with two 1 convolution to predict the four watershed levels.

We use a weighted cross-entropy loss to train this given by:

$$L_{wtr} = \sum_{k \in (0,3)} w_k W_k \log(p_k^{wtr}), \tag{4}$$

where W_k is the one-hot ground truth for k^{th} watershed level, p_k^{wtr} its predicted probability and w_k its weights.

3.4. Triplet Loss Network

The triplet loss network is used to refine and merge the detected candidate instance in addition to detecting new instances. Towards this goal, a popular choice is to formulate it as an embedding problem using triplet loss [5]. This loss forces features of pixels belonging to the same instance to group together while pushing apart features of pixels from different instances. Margin-separation loss is usually employed for better instance separation and is given by:

$$L(f_a, f_p, f_n) = \max\left((f_a - f_p)^2 - (f_a - f_n)^2 + \alpha, 0\right), \tag{5}$$

where f_a, f_p, f_n are the anchor, positive and negative pixel features *resp*. and α is the margin. Choosing α is not easy and depends on the complexity of the feature space [27]. Instead, here we opt for a two fully-connected network to classify the pixel features and formulate it as a binary classification problem:

$$T(f_a, f_*) = \begin{cases} 1 & \text{if, } f_* = f_p, \\ 0 & \text{if, } f_* = f_n, \end{cases} \tag{6}$$

Input	Blocks	Output
FPN	dc-256-256, dc-256-128	F_{ss}
F_{ss}	ups, cat, conv-512-(C_{stuff}+C_{thing}), ups	Segmentation
F_{ss}	2×dc-128-128	F_{hgh}
F_{hgh}	ups, cat, conv-512-128, conv-128-(4×C_{thing}), ups	Hough
F_{hgh}	2×dc-128-128	F_{wtr}
F_{wtr}	ups, cat, conv-512-128, conv-128-16, ups	F^*_W
F_{wtr}	2×dc-128-128	F_{trp}
F_{trp}	ups, cat, conv-512-128, conv-128-128, ups	F^*_T

Table 1. Architecture of BBFNet. *dc*, *conv*, *ups* and *cat* stand for deformable convolution [8], 1×1 convolution, upsampling and concatenation *resp*. The two numbers that follow *dc* and *conv* are the input and output channels to the blocks.* indicates that more processing is done on these blocks as detailed in §3.3 and §3.4.

We use the cross-entropy loss to train this head.

$$L_{trp} = \sum_{c \in (0,1)} T_c \ \log(p_c^{trp}), \tag{7}$$

T_c is the ground truth one-hot label for the indicator function and p^{trp} the predicted probability.

The pixel feature used for this network is a concatenation of F_T (see Table 1), its normalised position in the image (x, y), and the outputs of the different heads (p^{seg}, p^{wtr}, $\hat{X}_{\text{off}}$, $\hat{Y}_{\text{off}}$, σ_x and σ_y).

3.5. Training and Inference

We train the whole network along with its heads in an end-to-end fashion using a weighted loss function:

$$L_{\text{total}} = \alpha_1 \, L_{ss} + \alpha_2 \, L_{hgh} + \alpha_3 \, L_{wtr} + \alpha_4 \, L_{trp}. \tag{8}$$

For the triplet loss network, training with all pixels is prohibitively expensive. Instead we randomly choose a fixed number of anchor pixels N_a for each instance. Hard positive examples are obtained by sampling from the farthest pixels to the object center and correspond to watershed level $k = 0$. For hard negative examples, neighbouring instances' pixels closest to the anchor and belonging to the same class are given higher weight. Only half of the anchors use hard example mining while the rest use random sampling.

We observe that large objects are easily detected by the watershed head while Hough voting based center prediction does well when objects are of the same scale. To exploit this observation, we detect large object candidates ($I_{L'}$) using connected components on the watershed predictions corresponding to $k \geq 1$ bins. We then filter out candidates whose predicted Hough center ($I^{\text{center}}_{L'}$) does not fall within their bounding boxes ($BB_{L'}$). These filtered out candidates are fragmented regions of occluded objects or false detections. Using the center pixel of the remaining candidates ($I_{L''}$) as anchors points, the triplet loss network refines them over the remaining pixels allowing us to detect fragmented regions while also improving their boundary predictions.

After the initial watershed step, the unassigned *thing* pixels corresponding to $k = 0$ and primarily belong to small instances. We use mean-shift clustering with fixed bandwidth (B) to predict candidate object centers, I_S^{center}. We then back-trace pixels voting for their centers to obtain the Hough predictions I_S.

Finally, from the remaining unassigned pixels we randomly pick an anchor point and test it with the other remaining pixels. We use this as candidates regions that are filtered (I_R) based on their Hough center predictions, similar to the watershed candidates. The final detections are the union of these predictions. We summarize these steps in algorithm 1 provided in the supplementary section §7.

4. Experiments

In this section we evaluate the performance of BBFNet and present the results we obtain. We first describe the datasets and the evaluation metrics used. In §4.1 we describe the implementation details of our network. §4.2 then discusses the performance of individual heads and how its combination helps improve the overall accuracies. We presents both the qualitative and quantitative results in §4.3 and give a brief analysis of the computational advantage of BBFNet over other methods. We end this section by presenting some of the failure cases in §4.4 and comparing them with other MoE+BB based approaches.

Datasets: The Cityscapes dataset [7] contains driving scenes with 2048×1024 resolution images recorded over various cities in Germany and Switzerland. It consists of 2975 densely annotated images training images and a further 500 validation images. For the panoptic challenge, a total of 19 classes are split into 8 *things* and 11 *stuff* classes.

Microsoft COCO [23] is a large scale object detection and segmentation dataset with over $118k$ training (2017 edition) and $5k$ validation images with varying resolutions. The labels consists of 133 classes split into 80 *things* and 53 *stuff*.

Evaluation Metrics: We benchmark using the Panoptic quality (PQ) measure which was proposed in [16]. This measure comprises of two terms, recognition quality (RQ) and segmentation quality (SQ), to measure individual performance on recognition and segmentation tasks:

$$\text{PQ} = \underbrace{\frac{\sum_{(\text{p,g}) \in \text{TP}} \text{IoU(p,g)}}{|\text{TP}|}}_{\text{SQ}} \underbrace{\frac{|\text{TP}|}{|\text{ TP}| + \frac{1}{2}|\text{FP}| + \frac{1}{2}|\text{FN}|}}_{\text{RQ}}, \tag{9}$$

where, IoU is the intersection-over-union measure, (p,g) are the matching predicted and ground-truth regions (> 0.5 IoU), TP, FP and FN are true-positive, false-positive and false-negative respectively.

4.1. Implementation Details

We use the pretrained ImageNet [10] models for ResNet50 and FPN and train the BBFNet head from scratch. We keep the backbone fixed for initial epochs before training the whole network jointly. In the training loss (*eq*. 8), we set $\alpha_1, \alpha_2, \alpha_3$ and α_4 parameters to 1.0, 0.1, 1.0 and 0.5 respectively, since we found this to be a good balance between the different losses. The mean-shift bandwidth is set to reduced pixels of $B = 10$ to help the Hough voting head detect smaller instances. In the watershed head, the number of training pixels decreases with K and needs to be offset by higher w_k. We found the weights $0.2, 0.1, 0.05, 0.01$ to work best for our experiments. Moreover, these weights help the network focus on detecting pixels corresponding to lower bins on whom the connected-component is performed. To train the triplet-loss network head we set the number of pixels per object $N_a = 1000$. For smaller instance, we sample with repetition so as to give equal importance to objects of all sizes.

To improve robustness we augment the training data by randomly cropping the images and adding alpha noise, flipping and affine transformations. Cityscapes dataset is trained with full resolution. For COCO, the longest edge of each image is resized to 1024 while keeping the aspect ratio same.

A common practice during inference is to remove prediction with low detection probability to avoid penalising twice (FP & FN) [41]. In BBFNet these correspond to regions with poor segmentation (class or boundary). We use the mean segmentation probability over the predicted region as the detection probability and filter regions with low probability (< 0.65). Furthermore, we also observe boundaries shared between multiple objects to be frequently predicted as different instances. We filter these by having a threshold (0.1) on the IoU between the segmented prediction and its corresponding bounding box.

4.2. Ablation studies

We conduct ablation studies here to show the advantage of each individual head and how BBFNet exploits them. Table 2 shows the results of our experiments on Cityscapes. We use the validation sets for all our experiements. We observe that watershed or Hough voting heads alone do not perform well. In the case of watershed head this is because performing connected component analysis on $k = 1$ level (as proposed in [3]) leads to poor segmentation quality (SQ). Note that performing the watershed cut at $k = 0$ is also not optimal as this leads to multiple instances that share boundaries being grouped into a single detection. By combining the Watershed head with a refining step from the triplet loss network we observe over 10 point improvement in accuracy.

On the other hand, the performance of the Hough voting head depends on the bandwidth B that is used. Fig. 3 plots its performance with varying B. As B increases from 5 to 20 pixels we observe an initial increase in overall PQ before it saturates. This is because while the performance increases on large objects ($> 10k$ pixels), it reduces on small ($< 1k$ pixels) and medium sized objects. However, we observe that at lower B it outperforms the Watershed+triplet loss head on smaller objects. We exploit this in BBFNet (see §3.5) by using the watershed+triplet loss head for larger objects while using Hough voting head primarily for smaller objects.

W	H	T	PQ	SQ	PQ_s	PQ_m	PQ_l
✓	✗	✗	44.4	75.7	1.3	24.1	57.9
✗	✓	✗	49.7	78.8	11.6	37.4	44.5
✓	✗	✓	55.3	**79.8**	10.2	44.4	72.0
✓	✓	✓	**56.3**	79.4	**12.4**	**47.2**	**72.5**

Table 2. Performance of different heads (W- Watershed, H- Hough Voting and T- Triplet Loss Network) on Cityscapes validation set. BBFNet exploits the complimentary performance of watershed (large objects $> 10k$ pixels) and Hough voting head (small objects $< 1k$ pixels) resulting in higher accuracy. PQ_s, PQ_m and PQ_l are the PQ scores for small, medium and large objects respectively.

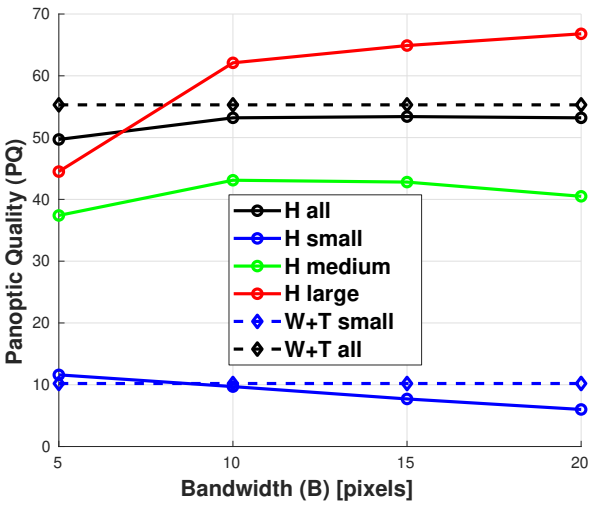

Figure 3. Performance of Hough voting head (H) with varying B for different sized objects, s-small $< 1k$ pixels, l-large $> 10k$ pixels and m-medium sized instances. For reference we also plot the performance of Watershed+Triplet loss (W+T) head (see Table 2).

4.3. Experimental Results

Table 3 benchmarks the performance of BBFNet with existing methods. As all state-of-the-art methods report results with ResNet50+FPN networks while using the same pre-training dataset (ImageNet) we also follow this convention and report our results with this setup. Multi-scale testing was used in some works but we omit those results here as this can be applied to any existing work includ-

ing BBFNet improving the predictions. From the result we observe that BBFNet, without using an MoE or BB, has comparable performance to other MoE+BB based methods while outperforming other non-BB based methods on most metrics. Fig. 4 shows some qualitative results on the Cityscapes validation dataset.

Method	BB	PQ	PQ_{Th}	PQ_{St}	IoU
FPSNet [9]	✓	55.1	48.3	60.1	-
TASCNet [19]	✓	55.9	50.5	59.8	-
AUNet [21]	✓	56.4	52.7	59.0	73.6
P. FPN [16]	✓	57.7	51.6	62.2	75.0
AdaptIS [35]	✓	59.0	55.8	61.3	75.3
UPSNet [41]	✓	59.3	54.6	62.7	75.2
Porzi *et al*. [28]	✓	**60.3**	**56.1**	**63.6**	**77.5**
DIN [20]	✗	53.8	42.5	62.1	71.6
SSAP [12]	✗	56.6	49.2	-	75.1
BBFNet	✗	56.3	49.7	61.0	76.2

Table 3. Panoptic segmentation results on the Cityscapes dataset. All methods use the same backbone of ResNet50+FPN with ImageNet pretraining. BBFNet is the only non-MoE method that does not use any instance detection, instance segmentation or proposal networks (BB). Bold is for overall best results and underscore is the best result in non-BB based methods.

In Table 4 we benchmark the quantitative performance on the Microsoft COCO dataset while qualitative results are shown in figure 6. Similar to the methodology used for Cityscapes we report results with same backbone and with same pre-training. We present results on individual classes in the supplementary material. BBFnet outperforms all exisiting non-BB methods while using a more efficient network backbone compared with others(ResNet50 vs ResNet101).

Method	BB	PQ	PQ_{Th}	PQ_{St}	IoU
AdaptIS [35]	✓	35.9	29.3	40.3	-
P. FPN [16]	✓	39.0	45.9	28.7	41.0
AUNet [21]	✓	39.6	49.1	25.2	45.1
TASCNet [19]	✓	40.7	47.0	31.0	-
UPSNet [41]	✓	**42.5**	**48.5**	**33.4**	54.3
DeepLab [42]	✗	33.8	-	-	-
SSAP [12]	✗	36.5	-	-	-
BBFNet	✗	37.1	42.9	28.5	**54.9**

Table 4. Panoptic segmentation results on Microsoft COCO-2017 dataset. All methods use the same backbone (ResNet50+FPN) and pretraining (ImageNet) except for SSAP (ResNet101) and DeepLab (Xception-71). Bold is for overall best results and underscore is the best result in non-BB based methods.

As BBFNet does not use a separate instance segmentation head, its computationally more efficient using only $\approx 28.6M$ parameters compared to $44.5M$ in UPSNet and $51.43M$ in [28]. We find a similar pattern when we compare the number of FLOPs on a 1024×2048 image with BBFNet taking 0.38 TFLOPs compared to 0.425 TFLOPs of UPSNet and 0.514 for [28]. Note that 0.28 TFLOPs correspond to the ResNet50+FPN backbone which is used in both methods making BBFNet 2.34 times more efficient in terms of FLOPs compared to [28].

To highlight BBFNets ability to work with different segmentation backbones we compare its generalisation with different segmentation networks. From table 5 we observe that BBFNets performance improves with better semantic segmentation backbones.

Network	Cityscapes				COCO			
	PQ	SQ	RQ	IoU	PQ	SQ	RQ	IoU
ERFNet [33]	47.8	77.2	59.7	69.8	-	-	-	-
ResNet50 [14]	56.3	79.4	69.1	76.2	37.1	77.6	45.2	54.9
ResNet101 [14]	**57.8**	**80.7**	**70.2**	**78.6**	**43.4**	**80.1**	**52.4**	**57.5**

Table 5. Panoptic segmentation results on Cityscapes and COCO datasets using different semantic segmentation backbones with BBFNet.

4.4. Error Analysis

We discuss the reasons for performance difference between our bounding-box free method and ones that use bounding-box proposals. UPSNet [41] is used as a benchmark as it shares common features with other methods. Table 6 depicts the number of predictions made for different sized objects in the Cityscapes validation dataset. We report the True Positive (TP), False Positive (FP) and the False Negative (FN) values.

Method	Small			Medium			Large		
	TP	FP	FN	TP	FP	FN	TP	FP	FN
UPSNet	1569	722	2479	3496	401	954	1539	49	82
BBFNet	1067	666	2981	3446	680	1004	1527	82	94

Table 6. Performance comparison of BBFNet with an MoE+BB method (UPSNet). Due to a non-MoE approach, errors from the backbone semantic segmentation network (low TP-small and high FP-medium,large) cannot be corrected by BBFNet.

One of the areas where BBFNet performs poorly is the number of small object detections. BBFNet detects $2/3$ of the smaller objects compared to UPSNet. Poor segmentation (wrong class label or inaccurate boundary prediction) also leads to a relatively higher FP for medium and large sized objects. Figure 5 shows some sample examples. The multi-head MoE approach helps addressing these issues but at the cost of additional complexity and computation time of Mask R-CNN as shown in §4.3. For applications where time or memory are more critical compared to detecting smaller objects, BBFNet would be a more suited solution.

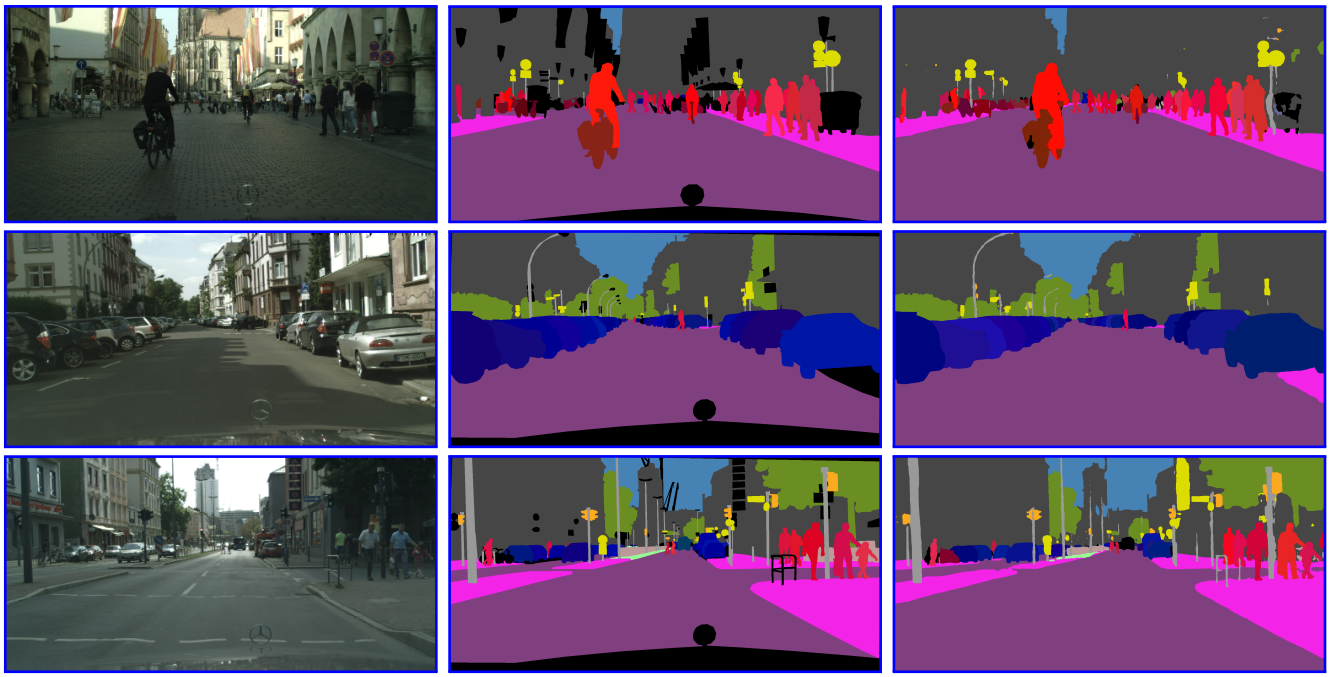

(a) Input Image (b) Ground truth (c) BBFNet predictions

Figure 4. Sample qualitative results of BBFNet on Cityscapes dataset. BBFNet is able to handle complex scenes with multiple occluded and fragmented objects.

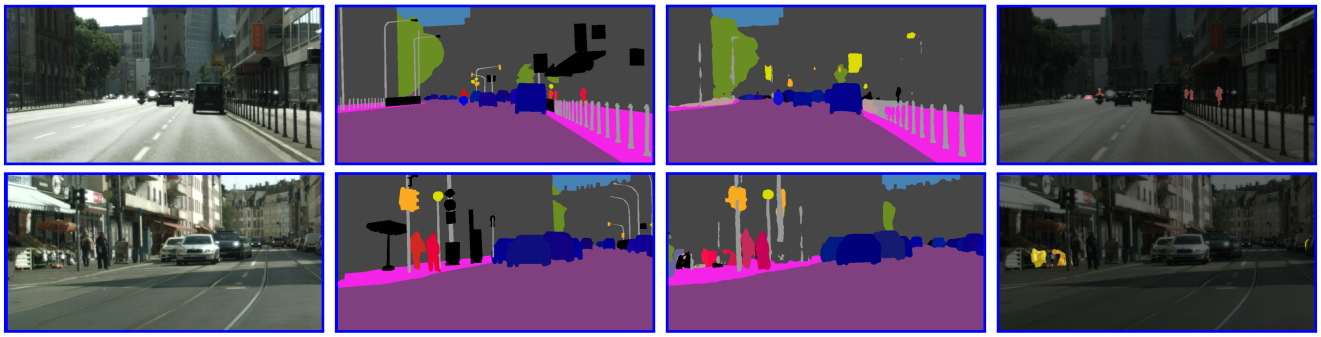

(a) Input Image (b) Ground truth (c) BBFNet predictions (d) Incorrect predictions

Figure 5. Sample results where BBFNet fails. First row shows an example where low confidence of semantic segmentation network leads to missed detection while the second row shows example of false positive due to wrong class label prediction. Without a MoE approach these errors from the semantic segmentation network cannot be corrected by BBFNet.

5. Conclusions and Future Work

We presented an efficient bounding-box free panoptic segmentation method called BBFNet. Unlike previous methods, BBFNet does not use any instance segmentation network to predict *things*. It instead refines the boundaries from the semantic segmentation output obtained from any off-the-shelf segmentation network. In this process we reduce the computational complexity while showing comparable performance with existing state-of-the-art methods in panoptic segmentation benchmarks.

In the next future we would like to improve the performance of BBFNet on small objects and to experiment with faster segmentation networks [29] towards the goal of expanding the capabilities of visual Simultaneous Localisation and Mapping (vSLAM) [24] with semantics and indi-

vidual object instances.

6. Acknowledgment

We would like to thank Prof. Andrew Davison and Alexandre Morgand for their critical feedback during the course of this work.

References

[1] D. Acuna, A. Kar, and S. Fidler. Devil is in the edges: Learning semantic boundaries from noisy annotations. In *IEEE Conf. on Computer Vision and Pattern Recognition (CVPR)*, pages 11075–11083, 2019. 3

[2] A. Arnab and P. H. Torr. Pixelwise instance segmentation with a dynamically instantiated network. In *IEEE Conf. on Computer Vision and Pattern Recognition (CVPR)*, 2017. 2

[3] M. Bai and R. Urtasun. Deep watershed transform for instance segmentation. In *IEEE Conf. on Computer Vision and Pattern Recognition (CVPR)*, pages 2858–2866, 2017. 2, 3, 4, 6

[4] D. H. Ballard. Generalizing the hough transform to detect arbitrary shapes. *Pattern Recognition*, 13(2):111–122, 1981. 3

[5] B. De Brabandere, D. Neven, and L. Van Gool. Semantic instance segmentation with a discriminative loss function. *arXiv preprint arXiv:arXiv:1708.02551*, 2017. 2, 3, 4

[6] Y. Cheng. Mean shift, mode seeking, and clustering. *IEEE Trans. Pattern Anal. Machine Intell.*, 17(8):790–799, 1995. 3

[7] M. Cordts, M. Omran, S. Ramos, T. Rehfeld, M. Enzweiler, R. Benenson, U. Franke, S. Roth, and B. Schiele. The cityscapes dataset for semantic urban scene understanding. In *IEEE Conf. on Computer Vision and Pattern Recognition (CVPR)*, 2016. 1, 5

[8] J. Dai, H. Qi, Y. Xiong, Y. Li, G. Zhang, H. Hu, and Y. Wei. Deformable convolutional networks. In *Intl. Conf. on Computer Vision (ICCV)*, 2017. 3, 5

[9] D. de Geus, P. Meletis, and G. Dubbelman. Fast panoptic segmentation network. *arXiv preprint arXiv:arXiv:1910.03892*, 2019. 2, 7

[10] J. Deng, W. Dong, R. Socher, L.-J. Li, K. Li, and L. Fei-Fei. ImageNet: A Large-Scale Hierarchical Image Database. In *IEEE Conf. on Computer Vision and Pattern Recognition (CVPR)*, 2009. 6

[11] D. Forsyth, J. Malik, M. Fleck, H. Greenspan, T. Leung, S. Belongie, C. Carson, and C. Bregler. Finding pictures of objects in large collections of images. In *Intl. workshop on object representation in computer vision*, 1996. 1

[12] N. Gao, Y. Shan, Y. Wang, X. Zhao, Y. Yu, M. Yang, and K. Huang. SSAP: Single-shot instance segmentation with affinity pyramid. In *Intl. Conf. on Computer Vision (ICCV)*, 2019. 2, 7

[13] K. He, G. Gkioxari, P. Dollár, and R. Girshick. Mask R-CNN. In *Intl. Conf. on Computer Vision (ICCV)*, 2017. 2

[14] K. He, X. Zhang, S. Ren, and J. Sun. Deep residual learning for image recognition. In *IEEE Conf. on Computer Vision and Pattern Recognition (CVPR)*, 2015. 7

[15] Y. Hu, Y. Zou, and J. Feng. Panoptic edge detection. *arXiv preprint arXiv:arXiv:1906.00590*, 2019. 3

[16] A. Kirillov, R. Girshick, K. He, and P. Dollár. Panoptic feature pyramid networks. In *IEEE Conf. on Computer Vision and Pattern Recognition (CVPR)*, 2019. 1, 2, 5, 7

[17] A. Kirillov, K. He, R. Girshick, C. Rother, and P. Dollár. Panoptic segmentation. In *IEEE Conf. on Computer Vision and Pattern Recognition (CVPR)*, 2019. 1, 2

[18] L. Ladický, C. Russell, P. Kohli, and P. H. S. Torr. Associative hierarchical CRFs for object class image segmentation. In *IEEE Conf. on Computer Vision and Pattern Recognition (CVPR)*, pages 739–746, 2009. 2

[19] J. Li, A. Raventos, A. Bhargava, T. Tagawa, and A. Gaidon. Learning to fuse things and stuff. *arXiv preprint arXiv:arXiv:1812.01192*, 2019. 2, 7

[20] Q. Li, A. Arnab, and P. H. Torr. Weakly-and semi-supervised panoptic segmentation. In *Eur. Conf. on Computer Vision (ECCV)*, 2018. 2, 7

[21] Y. Li, X. Chen, Z. Zhu, L. Xie, G. Huang, D. Du, and X. Wang. Attention-guided unified network for panoptic segmentation. In *IEEE Conf. on Computer Vision and Pattern Recognition (CVPR)*, 2019. 2, 7

[22] T. Lin, P. Goyal, R. Girshick, K. He, and P. Dollár. Focal loss for dense object detection. *IEEE Trans. Pattern Anal. Machine Intell.*, 2018. 2

[23] T. Lin, M. Maire, S. Belongie, J. Hays, P. Perona, D. Ramanan, P. Dollár, and C. L. Zitnick. Microsoft COCO: Common objects in context. In *Eur. Conf. on Computer Vision (ECCV)*, 2014. 1, 5

[24] J. McCormac, R. Clarck, M. Bloesch, S. Leutenegger, and A. J. Davison. Fusion++: Volumetric Object-Level SLAM. In *Intl. Conf. on 3D Vision (3DV)*, 2018. 8

[25] G. Neuhold, T. Ollmann, S. R. Bulò, and P. Kontschieder. The Mapillary Vistas dataset for semantic understanding of street scenes. In *Intl. Conf. on Computer Vision (ICCV)*, 2017. 1

[26] D. Neven, B. De Brabandere, S. Georgoulis, M. Proesmans, and L. Van Gool. Fast scene understanding for autonomous driving. *arXiv preprint arXiv:arXiv:1708.02550*, 2017. 2

[27] D. Neven, B. D. Brabandere, M. Proesmans, and L. V. Gool. Instance segmentation by jointly optimizing spatial embeddings and clustering bandwidth. In *IEEE Conf. on Computer Vision and Pattern Recognition (CVPR)*, 2019. 3, 4

[28] L. Porzi, S. R. Bulò, A. Colovic, and Peter Kontschieder. Seamless Scene Segmentation. In *IEEE Conf. on Computer Vision and Pattern Recognition (CVPR)*, 2019. 1, 2, 7

[29] R. P. Poudel, U. Bonde, S. Liwicki, and C. Zach. ContextNet: Exploring context and detail for semantic segmentation in real-time. In *British Machine Vision Conf. (BMVC)*, 2018. 8

[30] J. Redmon, S. Divvala, R. Girshick, and A. Farhadi. You only look once: Unified, real-time object detection. In *IEEE Conf. on Computer Vision and Pattern Recognition (CVPR)*, 2016. 3

[31] J. Redmon and A. Farhadi. Yolov3: An incremental improvement. *arXiv preprint arXiv:arXiv:1804.02767*, 2018. 2

[32] S. Ren, K. He, R. Girshick, and J. Sun. Faster R-CNN: Towards real-time object detection with region proposal net-

works. In *Advances in Neural Information Processing Systems (NIPS)*, 2015. 3

[33] E. Romera, J. M. Álvarez, L. M. Bergasa, and R. Arroyo. ERFNet: Efficient Residual Factorized ConvNet for Real-Time Semantic Segmentation. In *IEEE Trans. on Intelligent Transportation Systems*, volume 19, pages 263–272, 2018. 7

[34] J. Shotton, J. Winn, C. Rother, and A. Criminisi. Textonboost for image understanding: Multi-class object recognition and segmentation by jointly modeling texture, layout, and context. *IEEE Trans. Pattern Anal. Machine Intell.*, 81(1):2–23, 2009. 2

[35] K. Sofiiuk, O. Barinova, and A. Konushin. Adaptis: Adaptive instance selection network. In *Intl. Conf. on Computer Vision (ICCV)*, 2019. 2, 7

[36] T. Lin, P. Dollár, R. Girshick, K. He, B. Hariharan, and S. Belongie. Feature pyramid networks for object detection. In *IEEE Conf. on Computer Vision and Pattern Recognition (CVPR)*, 2017. 3

[37] J. Tighe, M. Niethammer, and S. Lazebnik. Scene parsing with object instances and occlusion ordering. In *IEEE Conf. on Computer Vision and Pattern Recognition (CVPR)*, 2014. 1

[38] J. Uhrig, M. Cordts, U. Franke, and T. Brox. Pixel-level encoding and depth layering for instance-level semantic labeling. In *German Conference on Pattern Recognition (GCPR)*, 2016. 2

[39] L. Vincent and P. Soille. Watersheds in digital spaces: an efficient algorithm based on immersion simulations. *IEEE Trans. Pattern Anal. Machine Intell.*, 13(6):583–598, 1991. 3

[40] K. Q. Weinberger and L. K. Saul. Distance metric learning for large margin nearest neighbor classification. *J. of Machine Learning Research*, 2009. 3

[41] Y. Xiong, R. Liao, H. Zhao, R. Hu, M. Bai, E. Yumer, and R. Urtasun. UPSNet: A unified panoptic segmentation network. In *IEEE Conf. on Computer Vision and Pattern Recognition (CVPR)*, 2019. 2, 6, 7

[42] T. Yang, M. Collins, Y. Zhu amd J. Hwang, T. Liu, X. Zhang, V. Sze, G. Papandreou, and L. Chen. Deeperlab: Single-shot image parser. *arXiv preprint arXiv:arXiv:1902.05093*, 2019. 7

[43] J. Yao, S. Fidler, and R. Urtasun. Describing the scene as a whole: joint object detection. In *IEEE Conf. on Computer Vision and Pattern Recognition (CVPR)*, 2012. 1

Algorithm 1 Compute Instance segments I

Require: Watershed levels W_k, predicted class c, probability p_c^{ss}, $\hat{X}_{\text{center}}$ and $\hat{Y}_{\text{center}} \vee c \in C_{thing}$

$I_{L'} \leftarrow$ connected-components on $W_k >= 1$. ▷*Large instance candidates*

$BB_{I_{L'}} \leftarrow$ bounding-box of $I_{L'}$.

$I_{L'}^{\text{center}} \leftarrow \frac{\sum_{x \in I_{L'}} \hat{X}_{\text{center}} p_c^{ss}}{\sum_{x \in I_{L'}} p_c^{ss}}, \frac{\sum_{y \in I_{L'}} \hat{Y}_{\text{center}} p_c^{ss}}{\sum_{y \in I_{L'}} p_c^{ss}}$.

$I_{L''} \leftarrow I_{L'}^{\text{center}} \in BB_{I_{L'}}$. ▷*Filter candidates*

$I_L \leftarrow I_{L''} \cup T(f_a, f_*) = 1 \vee f_a = I_{L''}^{\text{center}}$ & $f_* = c \in C_{thing}/I_{L''}$. 6

$I_S^{\text{center}} \leftarrow$ meanshift $\vee c \in C_{thing}/I_L$. ▷*Small instances*

$I_S \leftarrow$ Back-trace pixels voting for I_S^{center}

while $c \notin \emptyset$ **do** ▷*Remaining instances*

$I_{R'} \leftarrow (\cup T(f_a, f_*) = 1) \vee f_a =$ Random(c) & $f_* = c \in C_{thing}/I_L/I_S$. 6

end while

$BB_{I_{R'}} \leftarrow$ bounding-box of $I_{R'}$.

$I_{R'}^{\text{center}} \leftarrow \frac{\sum_{x \in I_{R'}} \hat{X}_{\text{center}} p_c^{ss}}{\sum_{x \in I_{R'}} p_c^{ss}}, \frac{\sum_{y \in I_{R'}} \hat{Y}_{\text{center}} p_c^{ss}}{\sum_{y \in I_{R'}} p_c^{ss}}$.

$I_R \leftarrow I_{R'}^{\text{center}} \in BB_{I_{R'}}$. ▷*Filter candidates*

$I \leftarrow I_L \cup I_S \cup I_R$

7. Supplementary

7.1. Inference Algorithm

We summarise the inference steps detailed in §3.5 in an algorithm 1

7.2. Cityscapes dataset

Table 7 gives the per-class results for the Cityscapes dataset. The first 11 classes are *stuff* while the rest 8 are *thing* label.

7.3. COCO dataset

Tables 8, 9 and 10 give the per-class results for the COCO dataset. The first 80 classes are *things* while the rest 53 are *stuff* label.

class	PQ	SQ	RQ	PQ_s	PQ_m	PQ_l
road	97.9	98.2	99.7	0.0	0.0	0.0
sidewalk	74.9	84.0	89.2	0.0	0.0	0.0
building	87.4	89.2	98.0	0.0	0.0	0.0
wall	26.2	72.0	36.4	0.0	0.0	0.0
fence	27.6	72.9	37.8	0.0	0.0	0.0
pole	50.8	65.2	77.9	0.0	0.0	0.0
T. light	40.7	68.4	59.4	0.0	0.0	0.0
T. sign	64.8	76.4	84.7	0.0	0.0	0.0
vegetation	88.3	90.3	97.8	0.0	0.0	0.0
terrain	27.6	72.4	38.1	0.0	0.0	0.0
sky	85.1	91.9	92.7	0.0	0.0	0.0
person	48.0	76.3	62.9	22.9	62.0	81.9
rider	43.8	71.2	61.6	11.2	54.3	71.7
car	64.7	84.5	76.5	32.2	72.2	91.5
truck	48.2	84.5	57.0	6.7	37.3	72.3
bus	69.1	88.5	78.1	0.0	49.6	85.0
train	46.1	80.7	57.1	0.0	10.7	64.2
motorcycle	36.9	72.5	50.9	8.9	44.3	56.6
bicycle	40.6	70.2	57.9	17.4	47.1	56.8

Table 7. Per-class results for cityscapes dataset. The first 11 classes are from *stuff* while the rest 8 are from *thing* label.

class	PQ	SQ	RQ	PQ_s	PQ_m	PQ_l
person	51.7	77.7	66.5	32.0	55.7	71.1
bicycle	17.6	66.9	26.4	7.9	19.5	33.2
car	42.1	81.0	52.0	30.9	54.9	56.0
motorcycle	40.6	74.1	54.8	13.7	35.7	58.9
airplane	56.8	78.0	72.7	45.4	37.5	72.3
bus	52.0	87.8	59.3	0.0	34.1	76.4
train	50.0	84.2	59.4	0.0	16.8	56.2
truck	24.3	78.4	31.0	13.3	21.5	36.7
boat	23.1	68.2	33.9	10.9	32.2	37.5
T. light	36.7	77.3	47.4	31.4	51.5	69.8
F. hydrant	77.5	87.1	88.9	0.0	71.6	91.3
S. sign	80.4	91.3	88.0	36.5	88.5	92.6
P. meter	56.2	87.9	64.0	0.0	48.6	82.0
bench	17.2	67.9	25.4	11.0	23.4	13.5
bird	28.2	73.5	38.4	15.0	47.5	78.6
cat	86.3	91.2	94.6	0.0	78.7	89.0
dog	69.3	86.0	80.6	0.0	58.5	82.9
horse	56.5	78.7	71.8	0.0	47.6	71.5
sheep	49.5	79.0	62.6	23.7	59.1	80.7
cow	42.3	82.5	51.4	0.0	32.4	70.1
elephant	63.0	83.9	75.0	0.0	37.4	71.5
bear	64.5	85.0	75.9	0.0	56.2	75.8
zebra	74.3	88.2	84.2	0.0	71.6	81.9
giraffe	73.1	82.2	88.9	0.0	77.0	72.4
backpack	9.6	83.5	11.5	2.8	16.4	34.7
umbrella	50.2	81.9	61.3	21.6	57.2	64.3
handbag	12.8	74.6	17.2	2.8	20.4	29.7
tie	29.8	77.6	38.5	0.0	56.2	51.4
suitcase	51.6	79.9	64.6	16.7	51.6	70.2
frisbee	70.4	85.8	82.1	51.1	77.7	93.0
skis	4.5	71.2	6.3	0.0	12.4	0.0
snowboard	24.2	65.3	37.0	9.5	34.3	0.0
kite	27.1	72.4	37.5	25.8	21.7	43.6
B. bat	23.8	67.9	35.0	35.0	8.5	0.0
B. glove	37.7	83.6	45.2	18.6	74.3	0.0
skateboard	37.3	71.5	52.2	0.0	48.8	50.6
surfboard	48.5	75.2	64.4	29.8	49.0	69.0
T. racket	58.1	83.0	70.0	27.1	68.6	86.7
bottle	38.6	80.7	47.8	29.5	49.4	81.8
wine glass	38.7	79.3	48.8	0.0	44.4	86.1
cup	48.5	88.1	55.0	15.9	70.9	75.6
fork	8.5	63.5	13.3	7.2	10.4	0.0
knife	17.7	78.7	22.5	0.0	26.3	68.2
spoon	20.2	76.4	26.4	0.0	36.9	0.0
bowl	29.9	78.6	38.0	17.3	32.2	39.8
banana	16.5	76.4	21.6	4.0	22.1	35.5
apple	30.4	87.5	34.8	8.0	63.6	51.3
sandwich	31.8	88.4	36.0	0.0	34.2	32.9
orange	59.8	88.3	67.7	36.1	37.9	82.8
broccoli	22.4	74.9	30.0	0.0	20.3	42.6
carrot	17.3	74.2	23.3	12.4	24.1	0.0
hot dog	26.5	68.6	38.6	13.7	29.6	27.5
pizza	44.5	83.2	53.5	12.6	37.5	54.5
donut	44.5	86.5	51.4	45.2	26.2	72.2

Table 8. Per-class results for COCO dataset. Continued in Table 9

class	PQ	SQ	RQ	PQ_s	PQ_m	PQ_l
cake	49.9	90.2	55.3	0.0	31.6	62.3
chair	24.0	74.3	32.3	7.4	33.6	41.5
couch	44.1	80.8	54.5	0.0	32.4	52.4
P. plant	27.2	74.1	36.7	16.6	33.1	27.3
bed	48.4	82.0	59.0	0.0	0.0	57.2
D. table	13.0	71.5	18.2	0.0	7.7	21.0
toilet	73.2	86.9	84.2	0.0	58.3	78.5
tv	57.2	86.8	66.0	0.0	49.4	72.2
laptop	57.2	81.7	70.0	0.0	44.0	67.9
mouse	68.2	86.6	78.8	44.3	81.0	62.6
remote	20.7	80.1	25.8	6.8	48.8	0.0
keyboard	52.4	85.2	61.5	0.0	46.8	72.2
cell phone	46.1	84.9	54.3	15.0	66.2	58.1
microwave	61.3	91.9	66.7	0.0	60.7	94.8
oven	33.3	79.1	42.1	0.0	19.5	42.4
toaster	0.0	0.0	0.0	0.0	0.0	0.0
sink	49.5	81.8	60.5	30.8	56.8	45.7
refrigerator	30.6	87.2	35.1	0.0	12.0	41.9
book	8.1	70.6	11.5	6.3	11.6	13.1
clock	59.3	86.4	68.7	40.9	68.1	92.5
vase	31.8	80.5	39.4	22.4	35.3	42.5
scissors	0.0	0.0	0.0	0.0	0.0	0.0
teddy bear	49.0	82.4	59.4	0.0	39.8	72.8
hair drier	0.0	0.0	0.0	0.0	0.0	0.0
toothbrush	0.0	0.0	0.0	0.0	0.0	0.0
banner	5.5	79.9	6.9	0.0	0.0	0.0
blanket	0.0	0.0	0.0	0.0	0.0	0.0
bridge	22.0	71.3	30.8	0.0	0.0	0.0
cardboard	16.6	75.7	21.9	0.0	0.0	0.0
counter	19.7	67.8	29.0	0.0	0.0	0.
curtain	45.6	83.0	54.9	0.0	0.0	0.0
door-stuff	24.4	72.8	33.6	0.0	0.0	0.0
floor-wood	35.5	82.7	43.0	0.0	0.0	0.0
flower	12.5	65.8	19.0	0.0	0.0	0.0
fruit	5.4	65.0	8.3	0.0	0.0	0.0
gravel	11.6	63.5	18.2	0.0	0.0	0.0
house	13.5	72.5	18.6	0.0	0.0	0.0
light	16.1	67.5	23.8	0.0	0.0	0.0
mirror-stuff	28.2	80.4	35.1	0.0	0.0	0.0
net	33.7	84.3	40.0	0.0	0.0	0.0
pillow	0.0	0.0	0.0	0.0	0.0	0.0
platform	10.3	92.5	11.1	0.0	0.0	0.0
playingfield	69.4	87.6	79.2	0.0	0.0	0.0
railroad	25.5	72.9	35.0	0.0	0.0	0.0
river	22.2	82.1	27.0	0.0	0.0	0.0
road	45.6	83.1	54.9	0.0	0.0	0.0
roof	5.2	80.8	6.5	0.0	0.0	0.0
sand	40.6	91.4	44.4	0.0	0.0	0.0
sea	71.0	91.6	77.5	0.0	0.0	0.0
shelf	8.8	76.3	11.5	0.0	0.0	0.0
snow	81.0	91.8	88.2	0.0	0.0	0.0
stairs	10.9	65.4	16.7	0.0	0.0	0.0
tent	5.3	53.3	10.0	0.0	0.0	0.0
towel	16.8	77.7	21.6	0.0	0.0	0.0

Table 9. Per-class results for COCO dataset. Continued in table 10

class	PQ	SQ	RQ	PQ_s	PQ_m	PQ_l
wall-brick	24.7	77.6	31.8	0.0	0.0	0.0
wall-stone	10.0	92.1	10.8	0.0	0.0	0.0
wall-tile	35.2	75.7	46.5	0.0	0.0	0.0
wall-wood	14.3	76.2	18.8	0.0	0.0	0.0
water-other	20.9	80.3	26.1	0.0	0.0	0.0
window-blind	44.6	84.7	52.6	0.0	0.0	0.0
window-other	22.2	73.7	30.0	0.0	0.0	0.0
tree-merged	64.6	80.7	80.0	0.0	0.0	0.0
fence-merged	19.7	74.9	26.3	0.0	0.0	0.0
ceiling-merged	57.3	81.8	70.1	0.0	0.0	0.0
sky-other-merged	76.9	90.4	85.1	0.0	0.0	0.0
cabinet-merged	33.1	79.7	41.5	0.0	0.0	0.0
table-merged	15.9	72.1	22.0	0.0	0.0	0.0
floor-other-merged	29.5	80.3	36.7	0.0	0.0	0.0
pavement-merged	36.4	78.9	46.2	0.0	0.0	0.0
mountain-merged	39.7	76.9	51.6	0.0	0.0	0.0
grass-merged	50.3	81.2	61.9	0.0	0.0	0.0
dirt-merged	27.4	77.0	35.6	0.0	0.0	0.0
paper-merged	4.7	74.6	6.3	0.0	0.0	0.0
food-other-merged	14.0	78.7	17.8	0.0	0.0	0.0
building-other-merged	29.3	76.4	38.4	0.0	0.0	0.0
rock-merged	31.0	78.4	39.6	0.0	0.0	0.0
wall-other-merged	45.6	79.2	57.6	0.0	0.0	0.0
rug-merged	38.3	82.7	46.4	0.0	0.0	0.0

Table 10. Per-class results for COCO dataset. The first 80 classes are from the *thing* while the rest 53 are from *stuff* label.

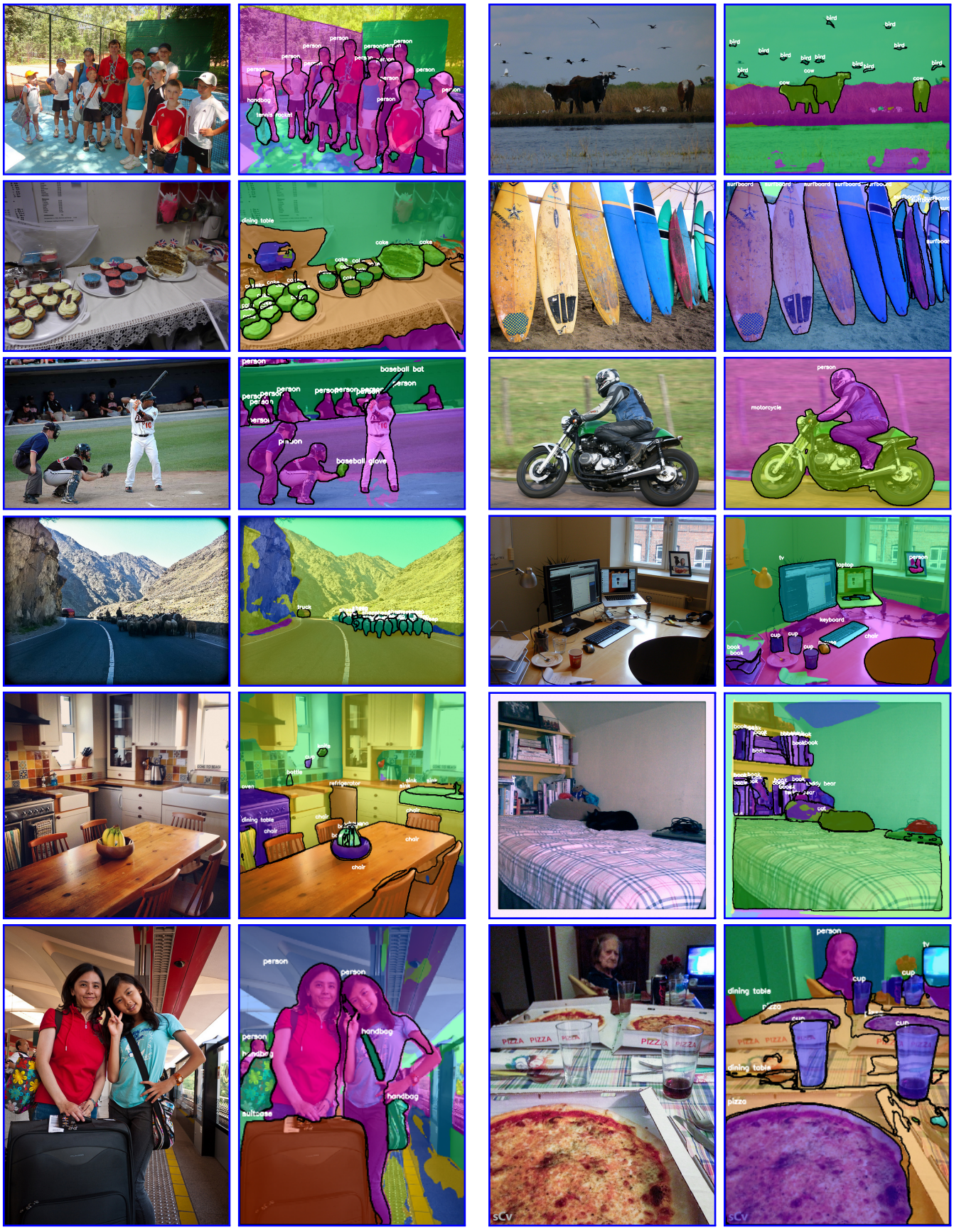

Figure 6. Sample qualitative results of BBFNet on COCO dataset. BBFNet can handle different object classes with multiple instances.